Available online at www.sciencedirect.com

ScienceDirect

Procedia Structural Integrity 18 (2019) 119–128

Structural Integrity Procedia

www.elsevier.com/locate/procedia

25th International Conference on Fracture and Structural Integrity

Investigation on fatigue strength of sand-blasted DMLS-AlSi10Mg alloy

Andrea Avanzini[a], Davide Battini[a], Marcello Gelfi[a], Luca Girelli[a], Candida Petrogalli[a], Annalisa Pola[a], Marialaura Tocci[a]*

[a] *Department of Mechanical and Industrial Engineering, University of Brescia, Via Branze 38, 25123, Brescia, Italy*

Abstract

Fatigue resistance of Direct Metal Laser Sintered (DMLS) AlSi10Mg alloy after sand-blasting was investigated in the present study. A preliminary characterization of the samples was carried out in order to identify material microstructure, surface roughness and superficial residual stresses. It was found that the applied post-processing treatment was responsible for a strong decrease in average surface roughness as compared to the as-built condition and induced compressive residual stresses on the samples surface. Axial fatigue tests were performed in both finite and infinite (i.e. $2x10^6$ cycles) life regimes and the obtained results were compared with literature values for the same alloy after various post-treatments, including heat treatment, machining, polishing and shot peening. A general positive effect of the applied sand-blasting on fatigue resistance was observed. This, coupled with the improvements of surface finishing, encourages the use of sand-blasting as a simple and effective post-treatment. Finally, observations of the fractured surfaces allowed also the identification of porosities located on the surface as the main crack initiation sites. Once the crack has started, it moves along a large flat area, as typical of fatigue propagation, with a small final overload region.

Peer-review under responsibility of the Gruppo Italiano Frattura (IGF) ExCo.

Keywords: DMLS; AlSi10Mg; Sand-blasting; Fatigue; Porosity

* Marialaura Tocci. Tel.: +39.030.3715415; fax: +39.030.3702448
E- address: m.tocci@unibs.it

2452-3216
Peer-review under responsibility of the Gruppo Italiano Frattura (IGF) ExCo.
10.1016/j.prostr.2019.08.146

1. Introduction

Additive Manufacturing (AM) represents a very attractive alternative to traditional processes in many industrial fields due to several potential advantages. These include the possibility to obtain near-net shaped components with complex geometries, even in small batches. Besides the production of prototypes or spare parts, AM processes are particularly suitable to develop lightweight structures (i.e. derived from topological optimization or generated by using lattice structures). This aspect is especially interesting for the application of Al alloys for AM in the automotive and aerospace sectors. Among Al alloys, the most widely used and studied is AlSi10Mg alloy, which is known to exhibit high tensile properties due to the extremely fine microstructure obtained by AM processes, as reported by Aboulkhair et al. (2015) and Read et al. (2015).

For structural applications, fatigue properties are also fundamental for a proper design (Nicoletto and Riva (2011)). In this regard, fatigue resistance of AlSi10Mg alloys has been characterized under various conditions. In fact, recent studies on fatigue properties of AM Al-Si alloys include investigations on the effect of process-related parameters, as such as building direction (Brandl et al. (2012); Uzan et al. (2017); Domfang Ngnekou et al. (2017)) or scanning strategy (Suryawanshi et al. (2016)). These authors focused on the influence of post-treatments, including heat treatments (involving platform heating and stress relief) (Brandl et al. (2012); Uzan et al. (2017); Aboulkhair et al. (2016)) and Hot Isostatic Pressing (HIP) (Siddique et al. (2015)), on fatigue resistance. Additionally, a significant role in determining fatigue properties is played by surface finishing. In fact, it is well known that defects close to the surface can be responsible for crack initiation during fatigue loading, as also found for AM Al-Si alloys (Brandl et al. (2012)).

Considering surface finishing, it should be mentioned that machining may help eliminating the influence of surface and subsurface condition on fatigue performance (Yadollahi and Shamsaei (2017)). In this way, it is possible to investigate the role of internal defects or porosities independently. Thus, many researchers opted for carrying out fatigue tests on machined samples, either to generate the reference fatigue data, which should then be modified with reduction factors when designing a component, or for comparison purposes. Among others, fatigue data for machined and/or polished AM-AlSi10Mg can be found in Brandl et al. (2012) for High Cycle Fatigue (HCF), in Romano et al. (2018) within the context of statistical analysis of defects, and in Uzan et al. (2017) and in Aboulkhair et al. (2016). Actually, a key advantage of additive manufacturing is the possibility to obtain (near)net shape components avoiding the need of machining operations, which could be also hardly feasible for some complex shapes. Therefore, it is important to assess the fatigue strength of the material in the as-built condition or after surface treatments not involving machining or polishing. At this regards, some studies considered different surface treatments, like sand-blasting or shot-peening (Uzan et al. (2018); Bagherifad et al. (2018); Damon et al. (2018)).

In Bagherifad et al. (2018) fatigue strength enhancement of Selective Laser Melted (SLM) AlSi10Mg parts by sand-blasting or shot-peening was studied, investigating synergetic effect with heat treatment. Sand-Blasting (SB) and Shot-Peening (SP) were demonstrated to remarkably improve fatigue strength compared to As-Built (AB) samples, whereas the synergetic effect of heat treatment was found to be different for AB, SB and SP specimens.

The effects of shot-peening on fatigue resistance of SLM AlSi10Mg specimens were also investigated in Uzan et al. (2018)**,** but considering different sequences of machining, polishing and shot-peening (with various types of balls). Surfaces polishing before shot-peening or following removal of about 25–30 μm from the surface after shot-peening showed improved fatigue resistance with an order of magnitude of about 100 MPa for treated samples.

In Damon et al. (2018)**,** the porosity distribution and morphology of selective laser melted samples for rotating bending test were investigated by means of micro-tomography analysis before and after shot-peening. Fatigue tests indicated the possibility to increase low and high-cycle-fatigue resistance after shot-peening.

In summary, surface post-treatments are recognized as a primary factor affecting fatigue and the usefulness of modifying the as-built surface has been suggested. Nevertheless, the current knowledge about its effectiveness is still incomplete. In the present study, the aim is the thorough investigation of fatigue properties of Direct Metal Laser Sintered (DMLS) AlSi10Mg alloy after sand-blasting only. In fact, as above discussed, post-processing treatments should be limited to the minimum to get the most advantage from AM, and SB is a convenient, easy and effective way to modify surface morphology.

In this contribution, axial fatigue tests were carried out and results were evaluated for both finite and infinite (i.e. $2x10^6$ cycles) life regimes. Reported results include the surface roughness analysis, determination of the residual stress state induced by sand-blasting, fatigue fracture surface analysis for identification of failure mechanism and a

preliminary investigation on defects on the transversal section of the specimens in order to correlate the failure to the microstructural quality.

2. Materials and methods

2.1. Additive manufacturing and sand-blasting parameters

The additive manufactured AlSi10Mg samples for both tensile and fatigue tests were produced with Direct Metal Laser Sintering technique on an EOS M290 system (400 W, Yb laser fibre; F-theta lens; 30 A and 400 V power supply; 7000 hPa, 20 m^3/h inert gas supply; 100 µm focus diameter; EOS GmbH Electro Optical System, EOS GmbH Electro Optical System, 2019).

Specimens were built in the vertical direction (z) with a layer thickness of 30 µm and an argon atmosphere, using the commercial EOS Aluminum AlSi10Mg powder. The preheating temperature of the building platform was set to 80 °C. The nominal composition of the samples is presented in Table 1.

Table 1. Nominal chemical composition (wt. %) of the studied alloy.

	Si	Mg	Fe	Cu	Mn	Ni	Zn	Pb	Sn	Ti	Al
Content (wt. %)	9 - 11	0.2-0.45	< 0.55	< 0.05	< 0.45	< 0.05	< 0.10	< 0.05	< 0.10	< 0.15	balance

The additive manufactured samples were manually sand-blasted using the B120 Microblast Ceramic Beads of Saint-Gobain Zirpro at a distance of about 10 cm from the nozzle and for an exposure time of 2 min at 0.5 MPa. The B120 particles presented a size distribution between 63 µm and 125 µm. The chemical analysis of the particles, performed by the producer, is reported in Table 2.

Table 2. Composition of particles used for sand-blasting.

	Minimum (%)	Maximum (%)
ZrO_2	60	70
SiO_2	28	33
Al_2O_3	0	10

2.2. Specimen Geometry

The geometry of the specimens used for tensile and fatigue tests is reproduced in Fig. 1.

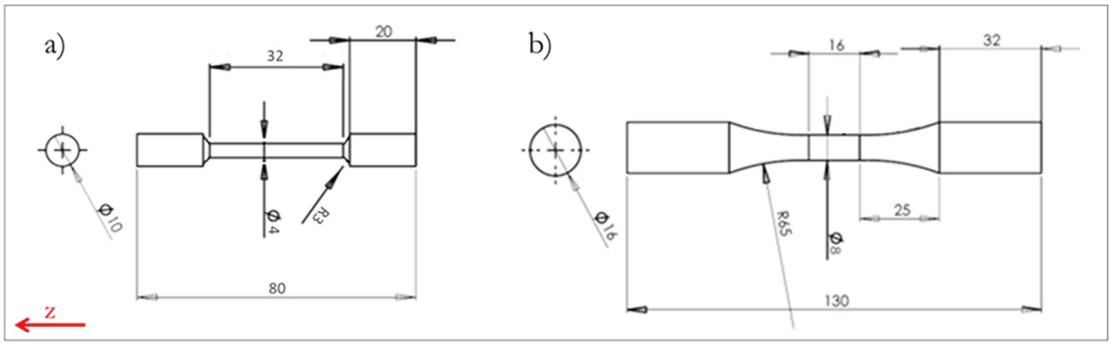

Fig. 1. Specimen geometry for (a) tensile test and (b) fatigue test.

A preliminary metallographic analysis of the samples was performed by means of a Leica DMI 5000M optical microscope and of a LEO EVO 40 scanning electron microscope (SEM). For microstructural observation, the specimens were cut perpendicularly as well as parallel to the building direction, polished up to mirror finishing and

etched with Keller's reagent (1% HF, 1.5% HCl, 2.5% HNO_3 and 95% H_2O) for 30 s, according to ASTM E407 standard.

Roughness measurements were performed using a stylus profilometer (Tribotechnique) equipped with a tip with radius of 5 μm on samples in as-built and sand blasted conditions. The track length was equal to 4.8 mm and the applied load to 1 mN. The measurement was repeated 5 times for each sample and average and standard deviation of roughness R_a was calculated. Filtering technique was set according to EN ISO 4287.

2.3. Test procedures

Tensile tests were performed on sand-blasted samples (Fig. 1a) using an Instron 3369 testing machine with a load cell of 50 kN. The elongation was monitored using a knife-edge extensometer (length of 25 mm) fixed to the gauge length of the specimens. Four specimens were tested at different crosshead speeds, corresponding to strain rates in the range 0.000167 - 0.015 s^{-1}.

The fatigue tests at different peak stress levels were performed on sand-blasted samples (Fig. 1b) with a load-controlled servo-hydraulic testing machine (Instron 8501) at room temperature (about 25 °C and 30 % relative humidity). The stress ratio R ($\sigma_{min}/\sigma_{max}$) was set to zero and the test frequency to 20 Hz. Eighteen tests were carried out and samples were loaded until the failure or until $2x10^6$ cycles were reached. Experimental data were processed according to the Standard ISO 12107. The stress and life were linearly interpolated in log-log coordinates and the fatigue strength was estimated via staircase method.

Since no prior knowledge of the fatigue behavior of the material was available, peak stress levels were selected to investigate fatigue strength for both finite and infinite (i.e. at $2x10^6$ cycles) life regimes. To this aim, the guidelines for S-N test method with a small sample size described in Lee et al. (2005) were followed. These are based on the method proposed in Nazakawa and Kodama (1987) for statistical evaluation of S-N, which requires:

- a minimum of 2 tests on 4 different stress levels for the finite fatigue life regime,
- a minimum of 6 tests for a simplified staircase for the infinite fatigue life regime.

Specifically, two fixed $\Delta\sigma$ were chosen: 12.5 MPa for the finite life curve and 5 MPa for the infinite life curve. From this set of data, the slope of the S-N curve in the finite life region can be calculated via linear regression and an estimate of fatigue strength can be obtained by applying a reduced staircase method.

The analysis of the fatigue fracture surfaces was carried out by means of a Leica DMS 300 digital microscope and a LEO EVO 40 scanning electron microscope.

Since sand-blasting is expected to modify the residual stress state in the surface, the experimental investigation included a comparative analysis of as-built and sand-blasted residual stresses measured by X-ray diffraction (XRD). The residual stress analysis was carried out on two specimens by using a Bruker D8 Discover XRD^2 diffractometer (Cu-Kα radiation) equipped with a beam collimator of 0.5 mm. The $\sin^2\psi$-method was applied in omega-mode configuration on the (331) plane of aluminum with tilting angle (psi) from -60 to 60°.

3. Results and discussion

3.1. Metallographic analysis

The microstructure of the additive manufactured samples is reported in Fig. 2.

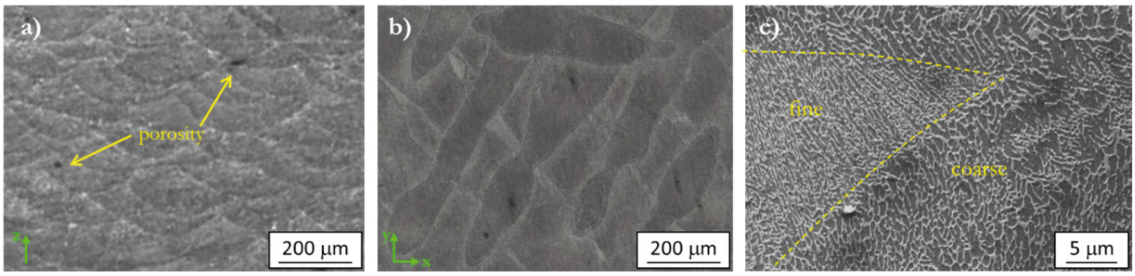

Fig. 2. Microstructure of additive manufactured sample after Keller's etching performed by optical microscopy in (a) vertical and (b) horizontal directions and (c) by scanning electron microscope.

The typical melting pools can be observed after Keller's etching, with the semi-spherical shape along the building direction (Fig. 2a) and elongated in the deposition plane (Fig. 2b), reflecting the laser beam movement during printing. Small porosities were found in the section because of the additive manufacturing technique, as reported also elsewhere (Louvis et al. (2011); Aboulkhair et al. (2014); Maskery et al. (2016); Frazler (2014); Ng et al. (2009); Girelli et al. (2019)).

The analysis performed by scanning electron microscope (Fig. 2c) showed Al-rich cellular grains surrounded by superfine Si particles (light network in Fig. 2c), coarser in the pools boundary than in the core, in agreement with the literature (Herzog et al. (2016); Wu et al. (2016); Cabrini et al. (2016)).

3.2. Specimen surface characterization

An example of the specimen surface appearance before and after sand-blasting is provided in Fig. 3.
No satellites or balling or porosity can be seen on the surface of the sand-blasted samples (Fig. 3b), contrary to the as-built ones (Fig. 3a) (Aboulkhair et al. (2016)). The repeated impact of hard particles during sand-blasting remarkably reduced the surface imperfections, even if somewhere emerging porosity can be detected.

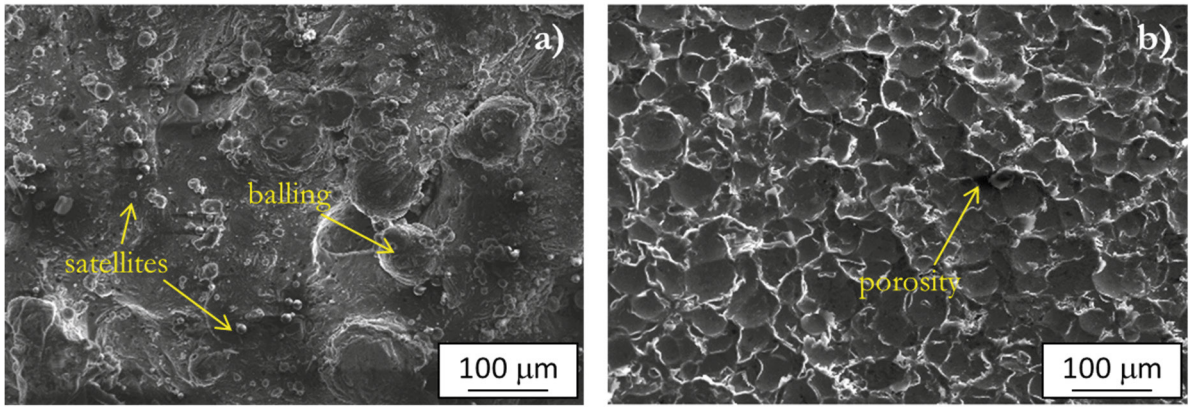

Fig. 3. Surface appearance of (a) as-built and (b) sand-blasted samples.

Average surface roughness R_a values are reported in Table 3. These confirm that the sand-blasting led to a significant decrease of surface roughness due to the removal of irregularities (satellites, balling or partially melted particles) from the surface, as visible in Fig. 3. Furthermore, the obtained results are in good agreement with surface roughness values reported by other authors (Bagherifad et al. (2018)) before and after sand-blasting. Despite the different sand-blasting parameters (mainly applied pressure and particles size), both in the present study and in Bagherifad et al. (2018), the post-treatment resulted in a surface roughness that is approximately the half as compared to the initial condition.

Table 3. Roughness measurements.

	R_a (µm)
As-built	13.2 ± 2.1
Sand-blasted	7.0 ± 1.2

3.3. Tensile tests

A summary of tensile test results is reported in Table 4. As apparent, no strain rate dependency could be observed for the range considered. By comparison with results published in Uzan et al. (2017); Aboulkhair et al. (2016); Mower and Long (2016), the tensile yield strength, the ultimate strength and the elastic modulus are very similar to data reported for as-built material.

Table 4. Results of tensile tests.

	Strain rates				
	0.0167% s^{-1}	0.03% s^{-1}	0.4% s^{-1}	1.5% s^{-1}	Average
Young Modulus [MPa]	57670	57600	57860	58870	58000±590
Ultimate strength [MPa]	421.5	418.9	406.7	381.5	407.2±18.3
Yield Strength [MPa]	254.4	252.9	246.54	248.6	250. 6±3.7

3.4. Residual stresses

On the as-built samples a tensile stress of 76 MPa ± 10 MPa and no shear stress were detected. This is related to the high cooling rates due to the peculiar manufacturing processes, as well documented in scientific literature (Li et al. (2018); Buchbinder et al. (2014)).

After sand-blasting, instead, the samples showed a compression residual stress of 105 MPa ± 2 MPa and no shear stress. It can be concluded that the applied sand-blasting successfully induced the presence of compressive residual stress likely due to a strain hardening mechanism induced by the repeated impact of hard particles on the sample surface (Wagner and Mueller (1992)). The effect of the mentioned post-treatment on residual stresses is believed to be positive for fatigue properties, as reported in other studies on AM AlSi10Mg alloy (Uzan et al. (2018); Bagherifad et al. (2018); Damon et al. (2018)). Furthermore, the obtained values are in good agreement with what found by other researchers on the surface of AlSi10Mg alloy in as-built and sand-blasted condition (Bagherifad et al. (2018)), even though this previous study reported a further increase in compressive stresses up to approximately 150 MPa at 0.1 mm from the surface.

3.5. Fatigue tests

The results of fatigue tests are summarized in Fig. 4, in the form of a traditional S_{max}-N curve with log-log coordinates with S_{max} being the peak stress of the loading cycle. Fig. 4 shows both the experimental data and the average regression curve with its lower confidence limit (LCL) determined with a Bayesian approach as the probability of 90% of the future population to fail with a 90% confidence. Specifically, fatigue strength resulted approximately 96 MPa with a lower limit of 86 MPa. Furthermore, despite the relatively small number of specimens, the fatigue curve resulting from experimental data showed low dispersion.

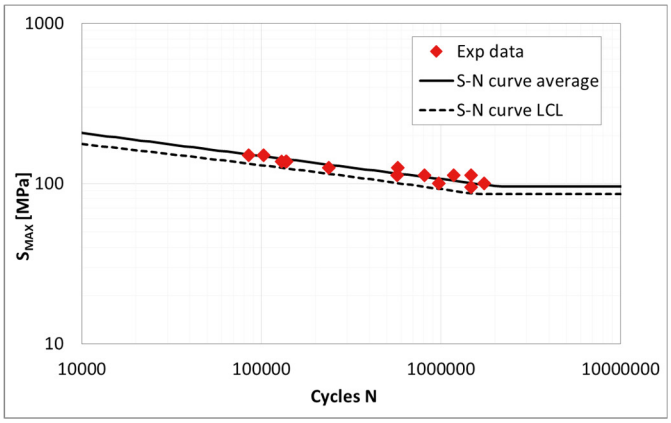

Fig. 4. Results of fatigue tests.

A comparison with published data can provide some interesting highlights, notwithstanding the variety of testing conditions reported and the number of processes and treatments involved.

Fatigue strength data for SLM AlSiMg10 were reported in the study by Aboulkhair et al. (2016) for specimens tested under uniaxial loading (R = 0.1) built in the Z direction, with or without machining and or heat treatment (HT). None of the as-built samples exceeded a pre-defined cut off limit at 3×10^7 cycles, even at the lowest maximum stress

level examined of 63 MPa, whereas for machined samples the same pre-defined cut off limit was reached at a maximum stress of 94 MPa. These results are really close to the fatigue strength observed in the present investigation with sand-blasting only. In the same study, slightly higher values of fatigue strength were reported for heat treated specimens.

Brandl et al. (2012) showed that both machining and T6 treatment lead to comparable, but slightly superior properties than the present case, while a significant increase is achieved changing the platform temperature.

Machined samples were also used in Tang and Pistorius (2017) for fatigue tests under uniaxial tension using a frequency of 50 Hz and a stress ratio R = 0.1. However, in this case, only two stress amplitudes S_a of 80 and 100 MPa were considered. Interestingly, for machined specimen built in the Z direction with S_a = 80 MPa, fatigue life was in the range 120000 - 190000 cycles, which is the same order of magnitude as life observed for sand-blasted specimen with S_a = 75 MPa in the present work.

The effects of surface treatment including shot-peening or sand-blasting on fatigue or synergetic effect with heat treatments were also investigated in literature. According to Bagherifad et al. (2018) sand-blasting and shot-peening remarkably improved fatigue strength, up to the range 160-176 MPa, but the synergetic effect of heat treatment was found to be different for as-built, sand-blasted or shot-peened specimens.

Especially in the case of sand-blasted condition Bagherifad et al. (2018), the higher fatigue strength in comparison with the present study can be due to the application of different sand-blasting parameters. In fact, they used abrasive particles of bigger size (200-300 μm Vs 60-155 μm) and a higher pressure (0.7 Vs 0.5 MPa), which could affect the number of superficial defects and irregularities as compared to the present work and resulting in different fatigue strength.

The effects of a sequence of treatments including machining, polishing and shot-peening on fatigue resistance of SLM- AlSi10Mg specimens were also investigated in Uzan et al. (2018). Specimen having their surfaces polished before shot-peening or removing about 25–30 μm from the surface after shot-peening showed improved fatigue resistance with a fatigue strength of about 100 MPa for treated samples.

When compared with the present study, fatigue limits reported in these papers are relatively higher. However, it should be noted that these investigations were carried out using fully reversed bending stresses, which is a different loading condition compared to axial testing.

Finally, numerical fitting of fatigue test data was also performed using Basquin's equation expressed as per eq. 1 (Stephens et al. (2001)):

$$S_a = A\,(N_f)^B \tag{1}$$

where S_a is the stress amplitude, N_f is the number of cycles to failure, and A and B are constants. Taking base-ten logarithms provides:

$$\mathrm{Log}(S_a) = \mathrm{Log}(A) + B\,\mathrm{Log}\,(N_f) \tag{2}$$

The experimental results for finite life of the present study could be generally well interpolated by a linear regression, with values of B and Log(A) equal to -0.13 ± 0.01 and 2.49 ± 0.08.

When compared with results reported in Aboulkhair et al. (2016) and Uzan et al. (2018), the value of B is relatively low, possibly indicating an improvement of fatigue performance.

Considering the differences between the various studies previously highlighted, our results confirm the usefulness of sand-blasting as a relatively simple treatment that may improve fatigue behavior of AM metal components.

The analysis of fracture surfaces has to be discussed in order to better understand the effect of the applied post treatment on the failure mechanism.

3.6. Fracture surface analysis

In general, the fracture surface analysis of fatigue samples observed at low magnification by digital microscope shows the presence of a large flat area, typical of fatigue propagation, with a small final overload region (Fig. 5). Additionally, several porosities can be noticed, as detected in the microstructural analysis (Fig. 2.3), both with

spherical shape (like those due to gas entrapment, melt splashing, etc. Louvis et al. (2011); Aboulkhair et al. (2014); Frazler (2014); Ng et al. (2009), and with irregular morphology (as such as lack of fusion or shrinkage porosity, as discussed in Girelli et al. (2019)

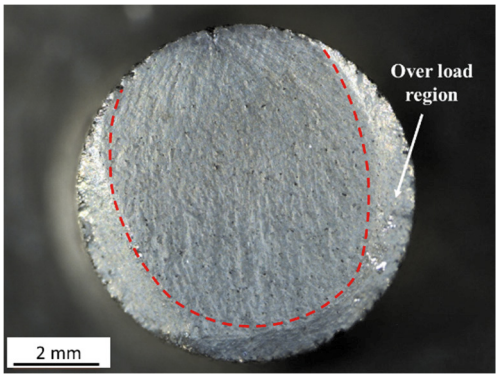

Fig. 5. Digital microscope image of fatigue fracture surface.

Observing the fracture surface at higher magnifications (Fig. 6-7), SEM analysis reveals that fatigue crack started from defects located at the surface. Furthermore, it is visible that the fracture initially moved very slowly in radial direction up to the distance indicated with a white dashed-line in Fig. 6a. After this slow initiation, the crack propagation became stable with the formation of the characteristic repetitive fatigue striations (Fig. 6b-c), which represent the crack propagation for each cycle of stress. The stress intensity at the crack tip progressively increased, accelerating the propagation rate, as also confirmed by the increase of fatigue striations inter-distance. This is evident if we compare these striations (Fig. 6c) with those in the regions near the end of the fatigue crack propagation (Fig. 6d). It is clear that the striations have a brittle appearance, as also reported by Aboulkhair et al. (2016) and attributed to the presence of high internal stresses developed in the AM sample during the rapid solidification.

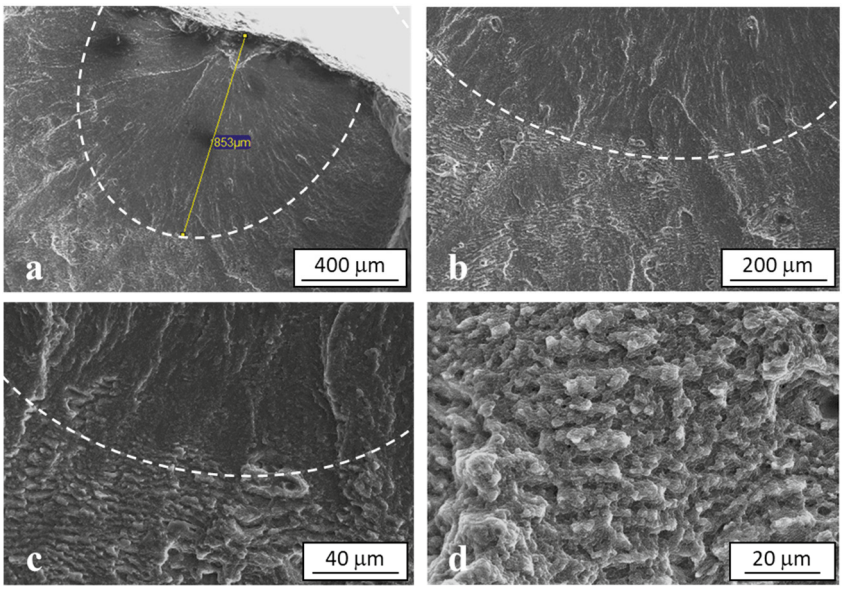

Fig. 6. SEM images of different areas on fatigue fracture surface: a-c) near the nucleation point and d) near the end of the crack propagation region

All the analyzed fatigue fracture surfaces show a single crack origin, starting from porosities and lack of fusion defects close to the surface (Fig. 7a-b), often coupled with poor surface roughness due to the formation of micro-depressions (Fig. 7c-d). These imperfections act as stress raisers, promoting the nucleation of fatigue crack. The images in Fig. 7c-d show that blasting has produced a small surface flattening effect, but not sufficient to significantly

improve the surface finishing. This is probably due to the limited size of particles used for sand-blasting in comparison with the large initial samples roughness.

It should be also mentioned that, in a previous work on the effect of sand blasting on fatigue mechanism Bagherifad et al. (2018), it was found that the fracture originated at sub-superficial defect. As above mentioned, this difference could be due to the higher sand particles size and pressure in comparison with the present work. This could have been more effective in removing superficial defects and closing open porosities, moving the crack initiation sites from superficial to sub-superficial defects. This despite the similar roughness values and superficial residual stresses measured after sand blasting.

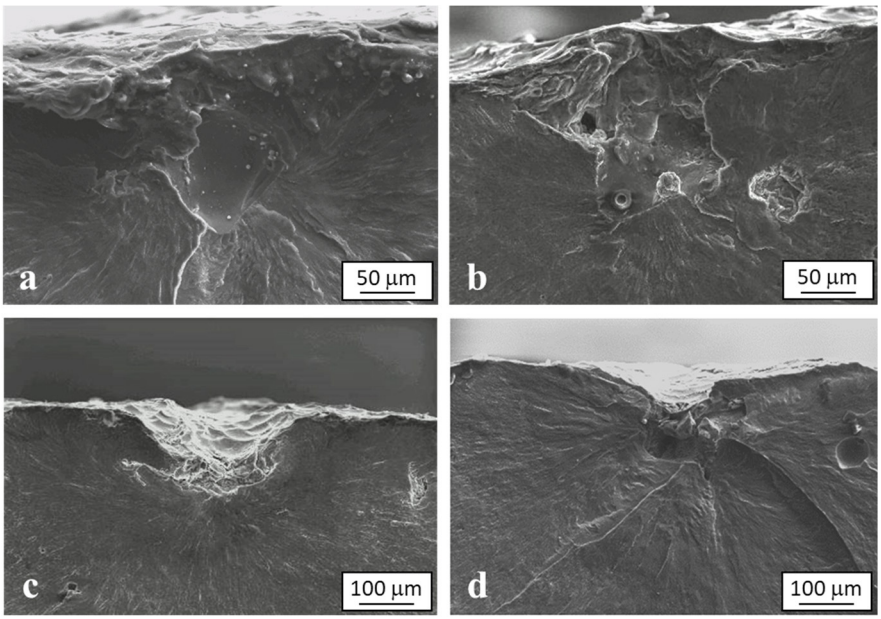

Fig. 7. SEM images of the fracture surface showing the typical defects which started the failure: a) porosities, b) lack of fusion defects, c-d) defects coupled with surface micro-depressions.

4. Conclusions

In the present study, axial fatigue tests were performed in order to study the fatigue behavior of AlSi10Mg samples produced by DMLS and, subsequently, sand-blasted. This post-processing treatment was found to be positive for fatigue properties in comparison with literature values regarding the same alloy in as-built condition or with various surface finishing. In fact, average surface roughness significantly decreased after sand-blasting due to the removal of defects and irregularities typical of the AM process, as demonstrated by SEM observation of the samples surface in as-built and sand-blasted conditions. Furthermore, XRD^2 measurements allowed the identification of a significant effect of this post treatment on superficial residual stresses. In fact, as-built samples were characterized by tensile residual stresses, while, after sand blasting, it was found that the surface was in a superficial compression state. This enhances fatigue resistance.

The investigation of the fracture mechanism by SEM detected the presence of superficial defects as crack initiation sites. This suggests that an optimization of sand blasting parameters could be helpful in further improving surface finishing, reducing the number of residual superficial irregularities, and, therefore, fatigue properties.

Acknowledgments

The authors wish to thank Bruker and Chem4Tech laboratory for the residual stress analysis, Dr. L. Montesano for

the support in SEM analysis.

References

Aboulkhair, N.T., Everitt, N.M., Ashcroft, I., Tuck, C., 2014. Reducing porosity in AlSi10Mg parts processed by selective laser melting. Additive Manufacturing 1, 77-86.

Aboulkhair, N.T., Maskery, I., Tuck, C., Ashcroft, I., Everitt, N.M., 2016. Improving the fatigue behaviour of a selectively laser melted aluminium alloy: Influence of heat treatment and surface quality. Mat. Des. 104, 174-182.

Aboulkhair, N.T., Tuck, C., Ashcroft, I., Maskery, I., Everitt, N.M., 2015. On the precipitation hardening of selective laser melted AlSi10Mg. Metallurgical and Materials Transactions A 46A, 3337-3341.

Bagherifad, S., Beretta, N., Monti, S., Riccio, M., Bandini, M., Guagliano, M., 2018. On the fatigue strength enhancement of additive manufactured AlSi10Mg parts by mechanical and thermal post-processing. Mat. Des. 145, 28-41.

Brandl, E., Heckenberger, U., Holzinger, V., Buchbinder, D., 2012. Additive manufactured AlSi10Mg samples using Selective Laser Melting (SLM): Microstructure, high cycle fatigue, and fracture behavior. Mater. Des. 34, 159-169.

Buchbinder, D., Meiners, W., Pirch, N., Wissenbach, K., 2014. Investigation on reducing distortion by preheating during manufacture of aluminum components using selective laser melting. Journal of Laser Applications 26, 012004.

Cabrini, M., Lorenzi, S., Pastore, T., Pellegrini, S., Manfredi, D., Fino, P., Biamino, S., Badini, C., 2016. Evaluation of corrosion resistance of Al–10Si–Mg alloy obtained bymeans of Direct Metal Laser SinteringMarina. Journal of Materials Processing Technology 231, 326-335.

Damon, J., Dietrich, S., Vollert, F., Gibmeier, J., Schulze, V., 2018. Process dependent porosity and the influence of shot peening on porosity morphology regarding selective laser melted AlSi10Mg parts. Additive Manufacturing 20, 77-89.

Domfang Ngnekou, J.N., Nadot, Y., Henaff, G., Nicolai, J., Ridosz, L., 2017. Influence of defect size on the fatigue resistance of AlSi10Mg alloy elaborated by selective laser melting (SLM. Procedia Structural Integrity 7, 75-83.

EOS GmbH Electro Optical System, 2019. EOS GmbH Electro Optical System. [Online] Available at: http://www.eos.info/eos-m290 [Accessed 29 March 2019].

Frazler, W.E., 2014. Metal Additive Manufacturing: A Review. JMEPEG 23, 1917-1928.

Girelli, L., Tocci, M., Gelfi, M., Pola, A., 2019. Study of heat treatment parameters for additively manufactured AlSi10Mg in comparison with corresponding cast alloy. Mat. Sci. Eng. A 739, 317-328.

Herzog, D., Seyda, V., Wycisk, E., Emmelmann, C., 2016. Additive manufacturing of metals. Acta Materialia 117, 371-392.

Lee, Y., Pan, J., Hathaway, R.B., Barkey, M.E., 2005. Fatigue Testing and Analysis, in. Elsevier, p.108.

Li, C., Liu, Z.Y., Fang, X.Y., Guo, Y.B., 2018. Residual Stress in Metal Additive Manufacturing. Procedia CIRP 71, 348-353.

Louvis, E., Fox, P., Sutcliffe, C.J., 2011. Selective laser melting of aluminium components. Journal of Materials Processing Technology 211(2), 275-284.

Maskery, I., Aboulkhair, N.T., Corfield, Tuck, C., Clare, Leach, R.K., Wildman, R.D., Ashcroft, I.A., Hague, , 2016. Quantification and characterisation of porosity in selectively laser melted Al–Si10–Mg using X-ray computed tomography. Materials Characterization 111, 193–204.

Mower, T.M.,Long, M.J., 2016. Mechanical behavior of additive manufactured, powder-bed laser-fused materials. Mat. Sci. Eng. A 651, 198-213.

Nazakawa, H., Kodama, S., 1987. Statistical S-N testing method with 14 specimens: JSME standard method for determination of S-N curve, in "Statistical Research on Fatigue and Fracture - Current Japanese Materials Research - Vol. 2". Tanaka T, Nishijima S, Ichikawa M Eds., pp.55.

Ng, G.K.L., Jarfors, A.E.W., Bi, G., Zheng, H.Y., 2009. Porosity formation and gas bubble retention in laser metal. Applied Physics A: Materials Science and Processing 97(3), 641-649.

Nicoletto, G., Riva, E., 2011. Elevated temperature fatigue behavior of cast aluminum alloys used for I.C. engine part production. Metall. Ital. 103(3), 41-48.

Read, N., Wang, W., Essa, K., Attallah, M.M., 2015. Selective laser melting of AlSi10Mg alloy: Process optimisation and mechanical properties development. Mater. Des. 65, 417-424.

Romano, S., Brückner-Foit, A., Brandão, A., Gumpinger, J., Ghidini, T., Beretta, S., 2018. Fatigue properties of AlSi10Mg obtained by additive manufacturing: Defect-based modelling and prediction of fatigue strength. Engineering Fracture Mechanics 187, 165-189.

Siddique, S., Imran, M., Rauer, M., Kaloudis, M., Wycisk, E., Emmelmann, C., Walther, F., 2015. Computed tomography for characterization of fatigue performance of selective laser melted parts. Mat. Des. 83, 661-669.

Stephens, R.I., Fatemi, A., Stephens, R.R., Fuchs, H.O., 2001. Metal Fatigue in Engineering, in. John Wiley & Sons.

Suryawanshi, J., Prashanth, K.G., Scudino, S., Eckert, J., Prakash, O., Ramamurty, U., 2016. Simultaneous enhancements of strength and toughness in an Al-12Si alloy synthesized using selective laser melting. Acta Mater. 115, 285-294.

Tang, M., Pistorius, P.C., 2017. Oxides, porosity and fatigue performance of AlSi10Mg parts produced by selective laser melting. International Journal of Fatigue 94, 192–201.

Uzan, N.E., Ramati, S., Shneck, R., Frage, N., Yeheskel, O., 2018. On the effect of shot-peening on fatigue resistance of AlSi10Mg specimens fabricated by additive manufacturing using selective laser melting (AM-SLM). Additive Manufacturing 21, 458-464.

Uzan, N.E., Shneck, R., Yeheskel, O., Frage, N., 2017. Fatigue of AlSi10Mg specimens fabricated by additive manufacturing selective laser melting (AM-SLM). Mat. Sci. Eng. A 704, 229-237.

Wagner, L. , Mueller, C., 1992. Effect of shot peening on fatigue behavior in al-alloys. Mater. Manuf. Process. 7, 423-440.

Wu, J., Wang, Wang, Attallah, Loretto, 2016. Microstructure and strength of selectively laser melted AlSi10Mg. Acta Materialia 117, 311-320.

Yadollahi, A., Shamsaei, N., 2017. Additive manufacturing of fatigue resistant materials: Challenges and opportunities. International Journal of fatigue, 98 (2017) 14-31 98, 14-30.